Numer. Math. (2014) 126:199–224
DOI 10.1007/s00211-013-0561-5

Numerische Mathematik

Generalized polarization tensors for shape description

Habib Ammari · Josselin Garnier · Hyeonbae Kang · Mikyoung Lim · Sanghyeon Yu

Received: 10 September 2012 / Revised: 18 February 2013 / Published online: 17 May 2013

Abstract With each domain, an infinite number of tensors, called the Generalized Polarization Tensors (GPTs), is associated. The GPTs contain significant information on the shape of the domain. In the recent paper (Ammari et al. in Math. Comput. **81**, 367–386, 2012), a recursive optimal control scheme to recover fine shape details of a given domain using GPTs is proposed. In this paper, we show that the GPTs can be used for shape description. We also show that high-frequency oscillations of the boundary of a domain are only contained in its high-order GPTs. Indeed, we provide an original

This work was supported by ERC Advanced Grant Project MULTIMOD-267184, National Research Foundation of Korea through Grants No. 2009-0070442, 2010-0017532 and 2010-0004091, and Posco TJ Park foundation.

H. Ammari (✉)
Department of Mathematics and Applications, Ecole Normale Supérieure, 45 Rue d'Ulm, 75005 Paris, France
e-mail: habib.ammari@ens.fr

J. Garnier
Laboratoire de Probabilités et Modèles Aléatoires & Laboratoire Jacques-Louis Lions, Université Paris VII, 75205 Paris Cedex 13, France
e-mail: garnier@math.jussieu.fr

H. Kang
Department of Mathematics, Inha University, Incheon 402-751, Korea
e-mail: hbkang@inha.ac.kr

M. Lim · S.Yu
Department of Mathematical Sciences, Korean Advanced Institute of Science and Technology, Daejeon 305-701, Korea
e-mail: mklim@kaist.ac.kr

S.Yu
e-mail: shyu@kaist.ac.kr

stability and resolution analysis for the reconstruction of small shape changes from the GPTs. By developing a level set version of the recursive optimization scheme, we make the change of topology possible and show that the GPTs can capture the topology of the domain. We also propose an indicator of topology which could be used in some particular cases to test whether we have the correct number of connected components in the reconstructed image. We provide analytical and numerical evidence that GPTs can capture topology and high-frequency shape oscillations. The results of this paper clearly show that the concept of GPTs is a very promising new tool for shape description.

Mathematics Subject Classification (2000) 35R30 · 35B30

1 Introduction

The aim of this paper is to propose a new tool for shape description. Our tool is based on the concept of generalized polarization tensors (GPTs) introduced in [9]. The concept of GPTs occurs in several interesting contexts, in particular, in asymptotic models of dilute composites (see [16,19,28]), in low-frequency scattering [7,8,14,21], in invisibility cloaking in the quasi-static regime [12] and in potential theory related to certain questions arising in hydrodynamics [29].

Another important use of this concept is for imaging diametrically small inclusions from boundary measurements. In fact, the GPTs are the basic building blocks for the asymptotic expansions of the boundary voltage perturbations due to the presence of small conductivity inclusions inside a conductor [5,23]. Based on this expansion, efficient algorithms to determine the location and some geometric features of the inclusions were proposed. We refer to [7,9] and the references therein for recent developments of this theory.

There are many methods for shape description and representation [27]. Of particular interest are the global scalar transform techniques which compute a scalar result based on the global shape. Moment based methods are among the most popular and well-known global scalar transform methods, see, for instance, [24,31], and [25].

In order to show the use of GPTs for shape description is an efficient global scalar transform technique, we first prove invariance properties of GPTs under translation, rotation, and scaling. Then we show that the GPTs capture high-frequency shape oscillations as well as topology. There is a (material) parameter in GPTs. It can be used as color so that GPTs can describe multiple connected domains with different colors. We also explicit the connection between the GPTs to the spectrum of the Neumann–Poincaré operator. To handle topology changes, we implement a level set version of the recursive matching GPTs algorithm introduced in [13]. We also give an indicator of topology which could be used in some particular cases to test whether we have the correct number of connected components in the reconstructed image. Moreover, we prove that high-frequency oscillations of the shape of a domain are only contained in its high-order GPTs and perform a stability and resolution analysis for the reconstruction of small shape changes from noisy GPTs. A generalization of the results of this paper to elastic GPTs [9,15] (also called elastic moment tensors) would

provide a new basis for shape description. This will be the subject of a forthcoming investigation.

2 Definition and basic properties of the GPTs

Throughout this paper we assume that the domains under consideration have $\mathcal{C}^2$-smooth boundaries and they are two dimensional. Let Γ be the fundamental solution to the Laplacian in two dimensions, *i.e.*,

$$\Gamma(x) = \frac{1}{2\pi} \ln |x|.$$

For a given bounded domain D in $\mathbb{R}^2$, the Neumann–Poincaré operator, $\mathcal{K}_D$, is defined for a density function $\phi \in L^2(\partial D)$ by

$$\mathcal{K}_D[\phi](x) = \frac{1}{2\pi} \int_{\partial D} \frac{\langle y - x, \nu(y) \rangle}{|x - y|^2} \phi(y)\, d\sigma(y), \quad x \in \partial D,$$

where $\nu(y)$ is the outward unit normal to ∂D at $y \in \partial D$ and $\langle\ ,\ \rangle$ denotes the scalar product in $\mathbb{R}^2$. Let $\mathcal{K}_D^*$ be the L^2-adjoint of $\mathcal{K}_D$, *i.e.*,

$$\mathcal{K}_D^*[\phi](x) = \frac{1}{2\pi} \int_{\partial D} \frac{\langle x - y, \nu(x) \rangle}{|x - y|^2} \phi(y)\, d\sigma(y).$$

It is well-known that for any real number λ with $|\lambda| > 1/2$ or $\lambda = -1/2$, $(\lambda I - \mathcal{K}_D^*)$ is invertible on $L^2(\partial D)$. Moreover, if $|\lambda| \geq 1/2$, then $(\lambda I - \mathcal{K}_D^*)$ is invertible on $L_0^2(\partial D) := \left\{ f \in L^2(\partial D) : \int_{\partial D} f d\sigma = 0 \right\}$. See, for instance, [22].

Let $|\lambda| > 1/2$. For a multi-index $\alpha = (\alpha_1, \alpha_2) \in \mathbb{N}^2$ where $\mathbb{N}$ is the set of all positive integers, define ϕ_α by

$$\phi_\alpha(y) := (\lambda I - \mathcal{K}_D^*)^{-1} \left[\nu(x) \cdot \nabla x^\alpha \right](y), \quad y \in \partial D. \tag{1}$$

Here and throughout this paper, we use the conventional notation: $x^\alpha = x_1^{\alpha_1} x_2^{\alpha_2}$, $|\alpha| = \alpha_1 + \alpha_2$.

The generalized polarization tensors (GPTs) $M_{\alpha\beta}$ for $\alpha, \beta \in \mathbb{N}^2$ ($|\alpha|, |\beta| \geq 1$) associated with the parameter λ and the domain D are defined by

$$M_{\alpha\beta}(\lambda, D) := \int_{\partial D} y^\beta \phi_\alpha(y) d\sigma(y). \tag{2}$$

The GPTs are the building blocks in representing the perturbation of the electrical potential in the presence of an inclusion D of conductivity contrast k. The parameter λ is related to k via the formula

$$\lambda = \frac{k+1}{2(k-1)}. \tag{3}$$

Note that the GPTs are real valued tensors. Key properties of positivity and symmetry of the GPTs are proved in [9, Chapter 4]. We emphasize that what is important is not the individual terms $M_{\alpha\beta}$ but their harmonic combinations. A harmonic combination of GPTs is $\sum_{\alpha,\beta} a_\alpha b_\beta M_{\alpha\beta}$ where $\sum_\alpha a_\alpha x^\alpha$ and $\sum_\beta b_\beta x^\beta$ are (real) harmonic polynomials. We call such (a_α) and (b_β) (real) harmonic coefficients. Let us recall the following symmetry property:

$$\sum_{\alpha,\beta} a_\alpha b_\beta M_{\alpha\beta}(\lambda, D) = \sum_{\alpha,\beta} a_\alpha b_\beta M_{\beta\alpha}(\lambda, D) \tag{4}$$

for any pair (a_α), (b_β) of harmonic coefficients. Moreover, the following uniqueness result holds [6].

Proposition 2.1 *If all harmonic combinations of GPTs of two domains are the same, i.e.,*

$$\sum_{\alpha,\beta} a_\alpha b_\beta M_{\alpha\beta}(\lambda_1, D_1) = \sum_{\alpha,\beta} a_\alpha b_\beta M_{\alpha\beta}(\lambda_2, D_2)$$

for all pairs (a_α), (b_β) of harmonic coefficients, then $D_1 = D_2$ and $\lambda_1 = \lambda_2$.

Proposition 2.1 says that the full knowledge of (harmonic combinations of) GPTs determines the domain D and λ. It is known that the first order GPT, $M_{\alpha\beta}$ for $|\alpha|+|\beta| = 2$, yields the equivalent ellipse [9,10]. The equivalent ellipse of D is the ellipse with same first order GPTs as D. However, it is not known analytically what kind of information on D and λ the higher order GPTs carry. It is the purpose of this paper to exploit the possibility of using higher order GPTs for the shape description.

In relation to the widely used shape description from moments, we recall the following result from [9, Theorem 4.13] which says that the GPTs can be estimated from above and below in terms of the harmonic moments.

Proposition 2.2 *Let $f(y) = \sum_{\alpha\in I} a_\alpha y^\alpha$ be a harmonic polynomial. Then*

$$\frac{2}{2\lambda+1}\int_D |\nabla f|^2 \le \sum_{\alpha,\beta\in I} a_\alpha a_\beta M_{\alpha\beta}(\lambda, D) \le \frac{2}{2\lambda-1}\int_D |\nabla f|^2 . \tag{5}$$

We also recall the following monotonicity of $\sum_{\alpha,\beta} a_\alpha a_\beta M_{\alpha\beta}(\lambda, D)$ with respect to the domain [11].

Proposition 2.3 *Let $D \subsetneqq D'$. Then, for all (nonzero) harmonic coefficients $(a_\alpha)_{|\alpha|\ge 1}$,*

$$\sum_{\alpha,\beta} a_\alpha a_\beta M_{\alpha\beta}(\lambda, D) < \sum_{\alpha,\beta} a_\alpha a_\beta M_{\alpha\beta}(\lambda, D') \quad \text{if } \lambda > \frac{1}{2},$$

and

$$\sum_{\alpha,\beta} a_\alpha a_\beta M_{\alpha\beta}(\lambda, D) > \sum_{\alpha,\beta} a_\alpha a_\beta M_{\alpha\beta}(\lambda, D') \quad \text{if } \lambda < -\frac{1}{2}.$$

Particularly interesting choices of harmonic coefficients are those of homogeneous harmonic polynomials: for a positive integer n and a multi-index α with $|\alpha| = n$, define (a_α^n) by

$$\sum_{|\alpha|=n} a_\alpha^n x^\alpha = r^n e^{in\theta} = (x_1 + ix_2)^n, \tag{6}$$

where $x = (r, \theta)$ in polar coordinates. Using these (complex) harmonic coefficients, we introduce for positive integers m and n

$$M_{mn}^c(\lambda, D) = \sum_{|\alpha|=m} \sum_{|\beta|=n} a_\alpha^m a_\beta^n M_{\alpha\beta}(\lambda, D). \tag{7}$$

We call M_{mn}^c the contracted GPTs [12]. An efficient algorithm for computing the contracted GPTs is presented in [18].

3 Translation, rotation, and scaling properties of the GPTs

In this section we show other properties of the GPTs which are particularly useful for shape description. Let N be a postitive integer. We prove that the set of $(M_{\alpha\beta}(\lambda, D))$ for $|\alpha| + |\beta| \le N$ is invariant under translation and rotation of D. We also provide a scaling formula for the GPTs.

3.1 Translation

For $T = (T_1, T_2)$, define $D^T := \{y + T : y \in D\}$ and $\partial D^T = (\partial D)^T$, and let $y^T = y + T$. For $\varphi \in L^2(\partial D)$, define $\varphi^T \in L^2(\partial D^T)$ as

$$\varphi^T(y^T) := \varphi(y), \quad \text{where } y \in \partial D.$$

Note that, for φ defined on ∂D, we have

$$\begin{aligned}
\mathcal{K}_{D^T}^*[\varphi^T](x^T) &= \frac{1}{2\pi} \int_{\partial D^T} \frac{\langle x^T - \tilde{y}, \nu(x^T)\rangle}{|x^T - \tilde{y}|^2} \varphi^T(\tilde{y})\, d\sigma(\tilde{y}) \\
&= \frac{1}{2\pi} \int_{\partial D} \frac{\langle x^T - y^T, \nu(x^T)\rangle}{|x^T - y^T|^2} \varphi^T(y^T)\, d\sigma(y) \\
&= \mathcal{K}_D^*[\varphi](x).
\end{aligned}$$

For multi-index α and γ, let the coefficients $c^T_{\alpha\gamma}$ be such that

$$(x - T)^\alpha = \sum_\gamma c^T_{\alpha\gamma} x^\gamma, \quad \forall\, x \in \mathbb{R}^2. \tag{8}$$

It is worth mentioning that $c^T_{\alpha\gamma} = 0$ if $|\gamma| > |\alpha|$.

Let $\varphi_{D,\alpha}$ be the density function defined by (1) for a given domain D and multi-index α. Then we have for $x^T \in \partial D^T$

$$\begin{aligned}\left(\lambda I - \mathcal{K}^*_{D^T}\right)[\varphi^T_{D,\alpha}](x^T) &= \left(\lambda I - \mathcal{K}^*_D\right)[\varphi_{D,\alpha}](x) \\ &= \nu(x) \cdot \nabla x^\alpha \Big|_{\partial D} \\ &= \sum_\gamma c^T_{\alpha\gamma} \nu(x^T) \cdot \nabla (x^T)^\gamma.\end{aligned}$$

Hence,

$$\varphi^T_{D,\alpha} = \sum_\gamma c^T_{\alpha\gamma} \varphi_{D^T,\gamma} \quad \text{on } \partial D^T,$$

and the following proposition holds.

Proposition 3.1 *Let $D^T = \{y + T : y \in D\}$. Then,*

$$M_{\alpha\beta}(\lambda, D) = \sum_{\eta,\gamma} c^T_{\beta\eta} c^T_{\alpha\gamma} M_{\eta\gamma}(\lambda, D^T), \tag{9}$$

where the coefficients $c^T_{\beta\eta}$ and $c^T_{\alpha\gamma}$ are given by (8).

Proof We compute

$$\begin{aligned}M_{\alpha\beta}(\lambda, D) &= \int_{\partial D} y^\beta \varphi_\alpha(y)\, d\sigma(y) \\ &= \int_{\partial D^T} (\tilde{y} - T)^\beta \varphi^T_{D,\alpha}(\tilde{y})\, d\sigma(\tilde{y}) \\ &= \int_{\partial D^T} \sum_\eta c^T_{\beta\eta} \tilde{y}^\eta \sum_\gamma c^T_{\alpha\gamma} \varphi_{D^T,\gamma}\, d\sigma(\tilde{y}),\end{aligned}$$

to find

$$M_{\alpha\beta}(\lambda, D) = \sum_{\eta,\gamma} c^T_{\beta\eta} c^T_{\alpha\gamma} M_{\eta\gamma}(\lambda, D^T),$$

as desired. □

For example, when $\alpha = (1, 0)$ and $\beta = (2, 0)$, we have $(x - T)^\alpha = x_1 - T_1$ and $(x - T)^\beta = (x_1 - T_1)^2 = x_1^2 - 2T_1x_1 + T_1^2$, and readily get

$$M_{(1,0),(2,0)}(\lambda, D) = M_{(1,0),(2,0)}(\lambda, D^T) - 2T_1 M_{(1,0),(1,0)}(\lambda, D^T).$$

3.2 Rotation

For $y \in \mathbb{R}^2$, let $y_\theta = \begin{pmatrix} \cos\theta & -\sin\theta \\ \sin\theta & \cos\theta \end{pmatrix} \begin{pmatrix} y_1 \\ y_2 \end{pmatrix}$, *i.e.*, the rotation of y with angle θ with respect to the origin. Set $D_\theta = \{y_\theta : y \in D\}$ and

$$\varphi^\theta(y_\theta) := \varphi(y), \quad y \in \partial D.$$

Note that, for a density function φ defined on ∂D, we have

$$\begin{aligned} \mathcal{K}^*_{D_\theta}[\varphi^\theta](x_\theta) &= \frac{1}{2\pi} \int_{\partial D_\theta} \frac{\langle x_\theta - \tilde{y}, \nu(x_\theta)\rangle}{|x_\theta - \tilde{y}|^2} \varphi^\theta(\tilde{y})\, d\sigma(\tilde{y}) \\ &= \frac{1}{2\pi} \int_{\partial D} \frac{\langle x_\theta - y_\theta, \nu(x_\theta)\rangle}{|x_\theta - y_\theta|^2} \varphi^\theta(y_\theta)\, d\sigma(y) \\ &= \mathcal{K}^*_D[\varphi](x). \end{aligned}$$

For multi-index α and γ, let the coefficients $r^\theta_{\alpha\gamma}$ be such that

$$(x_{-\theta})^\alpha = \sum_\gamma r^\theta_{\alpha\gamma} x^\gamma, \quad \forall x \in \mathbb{R}^2. \tag{10}$$

Again, it should be noted that $r^\theta_{\alpha\gamma} = 0$ if $|\gamma| \neq |\alpha|$. The following rotation formula for the GPTs can be proved in the same way as the translation formula (9).

Proposition 3.2 *Let $D_\theta = \{y_\theta : y \in D\}$. Then*

$$M_{\alpha\beta}(\lambda, D) = \sum_{\eta,\gamma} r^\theta_{\beta\eta} r^\theta_{\alpha\gamma} M_{\eta\gamma}(\lambda, D_\theta), \tag{11}$$

where the coefficients $r^\theta_{\beta\eta}$ and $r^\theta_{\alpha\gamma}$ are given by (10).

3.3 Scaling

Similarly, define for a positive real s, $D^s := \{sy : y \in D\}$ and set $\varphi^s(sy) = \varphi(y)$, $y \in \partial D$. Then, we have

$$\begin{aligned}\mathcal{K}^*_{D^s}[\varphi^s](x^s) &= \frac{1}{2\pi}\int_{\partial D^s}\frac{\langle x^s-\tilde{y},\nu(x^s)\rangle}{|x^s-\tilde{y}|^2}\varphi^s(\tilde{y})\,d\sigma(\tilde{y})\\ &= \frac{1}{2\pi}\int_{\partial D}\frac{\langle x^s-y^s,\nu(x^s)\rangle}{|x^s-y^s|^2}\varphi^s(y^s)s\,d\sigma(y)\\ &= \mathcal{K}^*_D[\varphi](x).\end{aligned}$$

From

$$(s^{-1}x)^\alpha = \frac{1}{s^{|\alpha|}}x^\alpha,\quad \forall\, x\in\mathbb{R}^2,$$

the following holds.

Proposition 3.3 *Let $D^s := \{sy :\ y\in D\}$ for a positive real number s. Then*

$$M_{\alpha\beta}(\lambda, D) = \frac{1}{s^{|\alpha|+|\beta|}}M_{\alpha\beta}(\lambda, D^s). \tag{12}$$

4 Shape derivative of the GPTs

Let $D = \cup_{j=1}^J D_j$ where D_j is a bounded connected domain with $\mathcal{C}^2$-boundary. To each D_j, we associate $|\lambda_j| > 1/2$ and set $\lambda = (\lambda_1,\dots,\lambda_J)$. The GPTs associated with the multiple inclusions $\cup_{j=1}^J D_j$ and λ can be defined similarly to the single inclusion case by using a system of integral equations; see Sect. 7. We emphasize that the translation, rotation, and scaling properties of the GPTs hold for multiple inclusions.

For ϵ small, let D_ϵ be an ϵ-deformation of D, *i.e.*, there are functions $h_j \in \mathcal{C}^1(\partial D_j)$, $1\le j\le J$, such that

$$\partial D_\epsilon := \cup_{j=1}^J\left\{\tilde{x} = x+\epsilon h_j(x)\nu_j(x)\ :\ x\in\partial D_j\right\}, \tag{13}$$

where ν_j is the outward unit normal vector on ∂D_j. Suppose that a_α and b_β are constants such that $H(x) = \sum_\alpha a_\alpha x^\alpha$ and $F(x) = \sum_\beta b_\beta x^\beta$ are harmonic polynomials. Then, according to [13], the perturbation of a harmonic sum of GPTs due to the shape deformation is given as follows:

$$\begin{aligned}&\sum_{\alpha,\beta}a_\alpha b_\beta M_{\alpha\beta}(\lambda, D_\epsilon) - \sum_{\alpha,\beta}a_\alpha b_\beta M_{\alpha\beta}(\lambda, D)\\ &\quad= \sum_{j=1}^J \epsilon(k_j-1)\int_{\partial D_j} h_j(x)\left[\frac{\partial u}{\partial\nu}\Big|_-\frac{\partial v}{\partial\nu}\Big|_- + \frac{1}{k_j}\frac{\partial u}{\partial T}\Big|_-\frac{\partial v}{\partial T}\Big|_-\right](x)\,d\sigma(x) + O(\epsilon^2),\end{aligned} \tag{14}$$

where $k_j = (2\lambda_j + 1)/(2\lambda_j - 1)$ and u and v are respectively solutions to the (primal and dual) problems:

$$\begin{cases} \Delta u = 0 & \text{in } D \cup (\mathbb{R}^2 \backslash \overline{D}), \\ u|_+ - u|_- = 0 & \text{on } \partial D_j,\ 1 \le j \le J, \\ \dfrac{\partial u}{\partial \nu}\Big|_+ - k_j \dfrac{\partial u}{\partial \nu}\Big|_- = 0 & \text{on } \partial D_j,\ 1 \le j \le J, \\ (u - H)(x) = O(|x|^{-1}) & \text{as } |x| \to \infty, \end{cases} \tag{15}$$

and

$$\begin{cases} \Delta v = 0 & \text{in } D \cup (\mathbb{R}^2 \backslash \overline{D}), \\ k_j v|_+ - v|_- = 0 & \text{on } \partial D_j,\ 1 \le j \le J, \\ \dfrac{\partial v}{\partial \nu}\Big|_+ - \dfrac{\partial v}{\partial \nu}\Big|_- = 0 & \text{on } \partial D_j,\ 1 \le j \le J, \\ (v - F)(x) = O(|x|^{-1}) & \text{as } |x| \to \infty. \end{cases} \tag{16}$$

The shape derivative of GPTs can be easily derived using (14), see Sect. 8.

5 Stability and resolution analysis in the linearized case

Let D be the unit disk, $|\lambda| > 1/2$, and $k = (2\lambda + 1)/(2\lambda - 1)$. Let $F(x) = r^m e^{im\theta}$ and $H(x) = r^n e^{in\theta}$ for $m, n \in \mathbb{N}$. The solutions u_n and v_m of respectively (15) and (16) are given by

$$u_n(x) = \begin{cases} \dfrac{2}{1+k} r^n e^{in\theta}, & r < 1, \\ \left(\dfrac{1-k}{1+k} \dfrac{1}{r^n} + r^n \right) e^{in\theta}, & r > 1, \end{cases}$$

and

$$v_m(x) = \begin{cases} \dfrac{2k}{1+k} r^m e^{im\theta}, & r < 1, \\ \left(\dfrac{1-k}{1+k} \dfrac{1}{r^m} + r^m \right) e^{im\theta}. & r > 1. \end{cases}$$

Let D_ϵ be an ϵ-perturbation of D:

$$\partial D_\epsilon := \{ \tilde{x} = x + \epsilon h(x) \nu(x) \ : x \in \partial D \},$$

where $h \in \mathcal{C}^1(\partial D)$. We use the Fourier convention

$$\hat{h}_p = \frac{1}{2\pi}\int_0^{2\pi} h(\theta)e^{-ip\theta}\,d\theta, \qquad h(\theta) = \sum_{p\in\mathbb{Z}} \hat{h}_p e^{ip\theta}.$$

Let $M^c_{mn}(\lambda, D_\epsilon)$ and $M^c_{mn}(\lambda, D)$ be the contracted GPTs associated with D_ϵ and D respectively. Since

$$\frac{\partial u_n}{\partial \nu}\Big|_- \frac{\partial v_m}{\partial \nu}\Big|_- + \frac{1}{k}\frac{\partial u_n}{\partial T}\Big|_- \frac{\partial v_m}{\partial T}\Big|_- = \frac{4(k-1)mn}{(k+1)^2} e^{i(m+n)\theta},$$

we obtain the following result.

Proposition 5.1 *We have*

$$M^c_{mn}(\lambda, D_\epsilon) - M^c_{mn}(\lambda, D) = 2\pi\epsilon\frac{mn}{\lambda^2}\hat{h}_{m+n} + O(\epsilon^2) \tag{17}$$

as $\epsilon \to 0$.

Proposition 5.1 shows that high-frequency oscillations of the boundary deformation of a disk-shaped inclusion are only contained in its high-order contracted GPTs. Moreover, only $\hat{h}_p$ for p up to $2N$ can be reconstructed from the set of contracted GPTs M^c_{mn} for $m, n \le N$.

Now, let δ be a small parameter. Following [4], we perform from (17) a stability and resolution analysis for the reconstruction of h from noisy $M^c_{mn}(\lambda, \delta D_\epsilon)$ for $m, n \le N$. For doing so, we introduce

$$a_{mn} = \frac{\lambda^2}{2\pi\,\delta^{m+n}}\left(M^c_{mn}(\lambda, \delta D_\epsilon) - M^c_{mn}(\lambda, \delta D)\right).$$

Assume that $M^c_{mn}(\lambda, \delta D_\epsilon)$ are corrupted with white noise. Thus,

$$a^{\text{meas}}_{m,n} = a_{mn} + \sigma W_{m,n},$$

with the noise terms $W_{m,n}$ modeled as independent standard complex circularly symmetric Gaussian random variables such that

$$\mathbb{E}[|W_{m,n}|^2] = e^{2\kappa(m+n)}, \tag{18}$$

σ thus modeling the noise magnitude and $\kappa := |\log\delta|$ describing its exponential growth as a function of m, n.

It follows from (12) and (17) that

$$a^{\text{meas}}_{m,n} = \epsilon mn\hat{h}_{m+n} + \sigma W_{m,n} + \epsilon^2 V^\epsilon_{m,n},$$

where $V^\epsilon_{m,n}$ denotes the approximation error. Therefore, introducing the estimator (for $p \ge 2$):

$$\hat{h}_p^{\text{est}} = \frac{1}{\epsilon} \sum_{n=1}^{p-1} \frac{1}{(p-n)n} a_{p-n,n}^{\text{meas}}$$

yields

$$\hat{h}_p^{\text{est}} = \hat{h}_p + \frac{\sigma}{\epsilon} \widetilde{W}_p + \epsilon \widetilde{V}_p^{\epsilon}, \tag{19}$$

with

$$\widetilde{W}_p = \sum_{n=1}^{p-1} \frac{1}{(p-n)n} W_{p-n,n}, \tag{20}$$

$$\widetilde{V}_p^{\epsilon} = \sum_{n=1}^{p-1} \frac{1}{(p-n)n} V_{p-n,n}^{\epsilon}. \tag{21}$$

Note that the independent standard complex circularly symmetric Gaussian random variables $\widetilde{W}_p$ are such that

$$\mathbb{E}[|\widetilde{W}_p|^2] = \left[\sum_{n=1}^{p-1} \frac{1}{n^2(p-n)^2} \right] \exp[2\kappa p] \overset{p \gg 1}{\simeq} \frac{\pi^2}{6p^2} \exp[2\kappa p]. \tag{22}$$

We assume that $\epsilon^2 \ll \sigma$, which insures that the measurement errors in the contracted GPTs dominate the approximation error, and introduce the signal-to-noise ratio (SNR):

$$\text{SNR} = \left(\frac{\epsilon}{\sigma} \right)^2.$$

Using (19) and (22) we obtain that the estimator $\hat{h}_p^{\text{est}}$ is unbiased:

$$\mathbb{E}[\hat{h}_p^{\text{est}}] = \hat{h}_p,$$

and has the following variance:

$$\mathbb{E}\left[|\hat{h}_p^{\text{est}} - \hat{h}_p|^2 \right] \simeq \frac{\pi^2}{6p^2} \text{SNR}^{-1} e^{2\kappa p}.$$

Following [4], one arrive using (19) and (22) at the following result.

Proposition 5.2 *Suppose that*

$$N < \frac{1}{2\kappa} \ln \text{SNR}, \tag{23}$$

and $\hat{h}_p$, $p \leq N$ are of order one. Then, the pth mode $\hat{h}_p$ of h, for $p \leq N$, can be resolved, i.e., $\mathbb{E}[|\hat{h}_p^{\text{est}} - \hat{h}_p|^2] < 1$.

Proposition 5.2 shows that a very high SNR is needed if one wishes to resolve the high order modes of the perturbation h. Furthermore, since κ is a decaying function of δ, we infer an expected result, that is, it is more difficult to estimate the high order modes of the perturbation h as the radius δ of the inclusion is smaller.

6 Spectrum of the Neumann–Poincaré operator and GPTs

Let $\mathcal{S}_D$ be the single-layer potential operator on ∂D defined for a density function $\phi \in L^2(\partial D)$ by

$$\mathcal{S}_D[\phi](x) = \frac{1}{2\pi} \int_{\partial D} \ln|x - y| \phi(y)\, d\sigma(y), \quad x \in \partial D.$$

It is well-known that the operator $-\mathcal{S}_D$ is a nonnegative operator. Moreover, the spectrum of the compact operator $\mathcal{K}_D^*$ lies in $]-1/2, 1/2]$. From [26] (see also [2]) there is a bounded self-adjoint (compact) operator A on $\text{Range}(\mathcal{S}_D)$ such that

$$A\sqrt{-\mathcal{S}_D} = \sqrt{-\mathcal{S}_D}\mathcal{K}_D^*. \tag{24}$$

Identity (24) is known as the symmetrization principle. Let P and $Q = I - P$ be the orthogonal projection from $L^2(\partial D)$ onto $\text{Ker}A$ and $(\text{Ker}A)^\perp$, respectively. Let $|\mu_1| \geq |\mu_2| \geq \cdots$ be the nonzero eigenvalues of A and Ψ_n be the corresponding normalized eigenfunctions. Let ϕ_α be the solution of (1). We have

$$\left(\lambda\sqrt{-\mathcal{S}_D} - \sqrt{-\mathcal{S}_D}\mathcal{K}_D^*\right)[\phi_\alpha] = \sqrt{-\mathcal{S}_D}\left[\frac{\partial x^\alpha}{\partial \nu}\right],$$

and hence,

$$(\lambda I - A)\sqrt{-\mathcal{S}_D}[\phi_\alpha] = \sqrt{-\mathcal{S}_D}\left[\frac{\partial x^\alpha}{\partial \nu}\right].$$

Therefore,

$$P\sqrt{-\mathcal{S}_D}[\phi_\alpha] = \frac{1}{\lambda} P\sqrt{-\mathcal{S}_D}\left[\frac{\partial x^\alpha}{\partial \nu}\right],$$
$$\lambda Q\sqrt{-\mathcal{S}_D}[\phi_\alpha] - AQ\sqrt{-\mathcal{S}_D}[\phi_\alpha] = Q\sqrt{-\mathcal{S}_D}\left[\frac{\partial x^\alpha}{\partial \nu}\right].$$

Consequently, using the spectral representation theorem we obtain that

$$Q\sqrt{-\mathcal{S}_D}[\phi_\alpha] = \sum \frac{\left\langle Q\sqrt{-\mathcal{S}_D}\left[\frac{\partial x^\alpha}{\partial \nu}\right], \Psi_n \right\rangle}{\lambda - \mu_n} \Psi_n, \tag{25}$$

where $\langle\ ,\ \rangle$ denotes the L^2 scalar product. Assume that the logarithmic capacity of ∂D is not 1 (see, for instance, [9, pp. 38–39]) and let f_β be the solution to

$$(-\mathcal{S}_D)[f_\beta] = y^\beta \quad \text{on } \partial D.$$

From the definition (2) of $M_{\alpha\beta}$ we obtain that

$$M_{\alpha\beta}(\lambda, D) = \int_{\partial D} (-\mathcal{S}_D)[f_\beta]\phi_\alpha \, d\sigma = \int_{\partial D} \sqrt{-\mathcal{S}_D}[f_\beta]\sqrt{-\mathcal{S}_D}[\phi_\alpha] \, d\sigma, \tag{26}$$

which yields the following proposition.

Proposition 6.1 *Assume that the logarithmic capacity of ∂D is not 1. The following representation of the GPTs in terms of the eigenvalues and the eigenvectors of the operator A defined by (24) holds:*

$$\begin{aligned} M_{\alpha\beta}(\lambda, D) = {} & \frac{1}{\lambda} \int_{\partial D} \left(P\sqrt{-\mathcal{S}_D}[f_\beta] \right) \left(P\sqrt{-\mathcal{S}_D} \left[\frac{\partial x^\alpha}{\partial \nu} \right] \right) \\ & + \sum_{n=1}^{\infty} \frac{1}{\lambda - \mu_n} \left\langle Q\sqrt{-\mathcal{S}_D} \left[\frac{\partial x^\alpha}{\partial \nu} \right], \Psi_n \right\rangle \langle Q\sqrt{-\mathcal{S}_D}[f_\beta], \Psi_n \rangle. \end{aligned} \tag{27}$$

7 GPTs of multiple connected domains

Let $D = \cup_{j=1}^J D_j$ be a cluster of inclusions. We assume that each D_j is a simply connected smooth domain. Let $\mathbb{K}^*$ be the Neumann–Poincaré operator corresponding to the cluster D of J well-separated inclusions:

$$\mathbb{K}^* := \begin{bmatrix} \mathcal{K}^*_{D_1} & \frac{\partial}{\partial \nu^{(1)}} \mathcal{S}_{D_2} & \cdots & \frac{\partial}{\partial \nu^{(1)}} \mathcal{S}_{D_J} \\ \frac{\partial}{\partial \nu^{(2)}} \mathcal{S}_{D_1} & \mathcal{K}^*_{D_2} & \cdots & \frac{\partial}{\partial \nu^{(2)}} \mathcal{S}_{D_J} \\ \vdots & \vdots & \ddots & \vdots \\ \frac{\partial}{\partial \nu^{(J)}} \mathcal{S}_{D_1} & \frac{\partial}{\partial \nu^{(J)}} \mathcal{S}_{D_2} & \cdots & \mathcal{K}^*_{D_J} \end{bmatrix}. \tag{28}$$

Here, $\nu^{(i)}$ denotes the outward normal to ∂D_i and $\mathcal{S}_{D_i}$ and $\mathcal{K}^*_{D_i}$ are the single layer and Neumann–Poincaré operator associated with D_i. From [10] it is known that there exists a unique solution to

$$(\lambda I - \mathbb{K}^*)[\Phi_\alpha](y) = \partial h_\alpha(y), \quad y \in \partial D,$$

where

$$\Phi_\alpha := \begin{bmatrix} \phi_\alpha^{(1)} \\ \vdots \\ \phi_\alpha^{(J)} \end{bmatrix}, \quad \partial h_\alpha(y) := \begin{bmatrix} \nu^{(1)}(y) \cdot \nabla y^\alpha \\ \vdots \\ \nu^{(J)}(y) \cdot \nabla y^\alpha \end{bmatrix},$$

and the GPTs of the cluster are defined by

$$M_{\alpha\beta}(\lambda, D := \cup_j D_j) := \sum_{j=1}^{J} \int_{\partial D_j} y^\beta \phi_\alpha^{(j)}(y) d\sigma(y).$$

As it has been said before, it is easy to see that the rotation, translation, and scaling properties proved in this paper for the GPTs can be generalized to those associated with multiple connected inclusions. On the other hand, it is proved in [3] that the symmetrization principle holds for $\mathbb{K}^*$, whose spectrum lies in $]-1/2, 1/2]$. Let $\mathbb{S}$ be given by

$$\mathbb{S} := \begin{bmatrix} \mathcal{S}_{D_1} & \mathcal{S}_{D_2} & \cdots & \mathcal{S}_{D_J} \\ \mathcal{S}_{D_1} & \mathcal{S}_{D_2} & \cdots & \mathcal{S}_{D_J} \\ \vdots & \vdots & \ddots & \vdots \\ \mathcal{S}_{D_1} & \mathcal{S}_{D_2} & \cdots & \mathcal{S}_{D_J} \end{bmatrix}. \tag{29}$$

Assume that $\mathrm{Ker}(\mathbb{S}) = \{0\}$ (which reduces when $J = 1$ to the fact that the logarithmic capacity of ∂D is not 1). Again from [3] we know that the eigenvalue $1/2$ of $\mathbb{S}\mathbb{K}^*$ has multiplicity J. Using this important fact, we obtain that

$$\Phi_\alpha = \frac{1}{\lambda - \frac{1}{2}} \sum_{j=1}^{J} \langle \partial h_\alpha, \mathbb{S}\theta_j \rangle \theta_j + \Phi_\alpha^\perp,$$

with $\Phi_\alpha^\perp$ being orthogonal (in $L^2(\partial D)$) to $\Phi_\alpha - \frac{1}{\lambda - \frac{1}{2}} \sum_{j=1}^{J} \langle \partial h_\alpha, \mathbb{S}\theta_j \rangle \theta_j$ and bounded (in $L^2(\partial D)$) as $\lambda \to \frac{1}{2}^+$. Here, θ_j, $j = 1, \ldots, J$, are orthonormal basis of the eigenspace associated with $1/2$.

The following result holds.

Proposition 7.1 *Assume that D is such that $Ker(\mathbb{S}) = \{0\}$. Then we have*

$$\lim_{\lambda \to \frac{1}{2}^+} \left(\lambda - \frac{1}{2}\right) M_{\alpha\beta}(\lambda, D) = \sum_{j=1}^{J} \langle \partial h_\alpha, \mathbb{S}\theta_j \rangle \langle x^\beta, \theta_j \rangle. \tag{30}$$

A few remarks are in order. First, we should note that it is known from [9] that $\sum a_\alpha M_{\alpha\beta}(\lambda, D)$ has a finite limit as $\lambda \to \frac{1}{2}^+$ provided that $\sum a_\alpha x^\alpha$ is a harmonic polynomial. This result can be seen here from the fact that

$$\left\langle \sum a_\alpha \partial h_\alpha, \mathbb{S}\theta_j \right\rangle = 0.$$

A second remark is about the application of (30) in order to detect the number J of connected components of the cluster. Assume that we have in hand $M_{\alpha\beta}(\lambda, D)$ for λ close to $1/2$ and α such that x^α is not harmonic and an initial guess $\cup_{j=1}^{J} D_j$ for D. Then

we compute the quantity $\sum_{j=1}^{J}\langle\partial h_\alpha, \mathbb{S}\theta_j\rangle\langle x^\beta, \theta_j\rangle$. From (30), it follows that if there is a large discrepancy between $(\lambda-\frac{1}{2})M_{\alpha\beta}(\lambda, D)$ and $\sum_{j=1}^{J}\langle\partial h_\alpha, \mathbb{S}\theta_j\rangle\langle x^\beta, \theta_j\rangle$, then the number of connected inclusions J may not be correct. Therefore, $(\lambda-\frac{1}{2})M_{\alpha\beta}(\lambda, D)$ may be used as an indicator of topology to check whether we have the correct number of connected inclusions.

8 GPTs matching approach

8.1 Minimization algorithm

Let D be an unknown domain, which could be a cluster of separated inclusions as in Sect. 4. We let $M_{\alpha\beta}(\lambda, D)$ denote the GPTs associated with $D = \cup_{j=1}^{J} D_j$ and $\lambda = (\lambda_1, \ldots, \lambda_J)$. Suppose that $M_{\alpha\beta}(\lambda, D)$ are known for all $|\alpha| + |\beta| \leq N$ for some number N. We reconstruct the location and the shape of D by minimizing the discrepancy between the given and simulated GPTs. In [13], a recursive algorithm to approximate the shape of D is proposed. The recursive optimization procedure is to minimize over B for $l = 3, \ldots, N$,

$$\mathcal{J}^{(l)}[B] := \frac{1}{2}\sum_{|\alpha|+|\beta|\leq l}\left|\sum_{\alpha,\beta} a_\alpha b_\beta M_{\alpha\beta}(\lambda, B) - \sum_{\alpha,\beta} a_\alpha b_\beta M_{\alpha\beta}(\lambda, D)\right|^2. \tag{31}$$

Here the coefficients (a_α) and (b_β) are such that $H(x) = \sum a_\alpha x^\alpha$ and $F(x) = \sum b_\beta x^\beta$ are homogeneous harmonic polynomials. At step l one uses as an initial guess the result of step $l-1$. At the first step ($l = 3$) one gets an equivalent ellipse as well as the location of the domain [13].

Note that using definition (7) of the contracted GPTs, one can see that minimizing $\mathcal{J}^{(l)}$ is equivalent to minimizing

$$\mathcal{J}_c^{(l)}[B] := \frac{1}{2}\sum_{n+m\leq l}\left|M_{nm}^c(\lambda, B) - M_{nm}^c(\lambda, D)\right|^2. \tag{32}$$

To minimize $\mathcal{J}^{(l)}[B]$ we need to compute the shape derivative, $d_S\mathcal{J}^{(l)}$, of $\mathcal{J}^{(l)}$, which it can be obtained easily using (14). Suppose that B has J' components, *i.e.*, $B = \cup_{j=1}^{J'} B_j$, and the conductivity of B_j is k_j. Let $h = (h_1, \ldots, h_{J'})$ be the functions determining the deformation of ∂B_j, $j = 1, \ldots, J'$. Let

$$w_j^{HF}(x) = (k_j - 1)\left[\frac{\partial u}{\partial \nu}\Big|_- \frac{\partial v}{\partial \nu}\Big|_- + \frac{1}{k_j}\frac{\partial u}{\partial T}\Big|_- \frac{\partial v}{\partial T}\Big|_-\right](x), \quad x \in \partial B_j$$

where u and v satisfy (15) and (16) with D replaced by B, respectively. From (14) the shape derivative of $\mathcal{J}^{(l)}$ at B in the direction of h is given by

$$\left\langle d_S \mathcal{J}^{(l)}[B], h \right\rangle = \sum_{|\alpha|+|\beta|\le l} \delta_{HF} \sum_{j=1}^{J'} \left\langle w_j^{HF}, h_j \right\rangle_{L^2(\partial B_j)}, \tag{33}$$

where

$$\delta_{HF} = \sum_{\alpha,\beta} a_\alpha b_\beta \left(M_{\alpha\beta}(\lambda, B) - M_{\alpha\beta}(\lambda, D) \right).$$

It is worth mentioning that the only information about h_j which is used in formula (33) is the projections onto the space spanned by w_j^{HF}.

If the target domain D is connected (and consequently all the domains B under consideration are connected), one can modify the earlier shape B to obtain B^{mod} for the next step by applying the gradient descent method:

$$\partial B^{\text{mod}} = \partial B - \left(\frac{\mathcal{J}^{(l)}[B]}{\sum_{H,F} \left(\langle d_S \mathcal{J}^{(l)}[B], w^{HF} \rangle \right)^2} \sum_{H,F} \langle d_S \mathcal{J}^{(l)}[B], w^{HF} \rangle w^{HF} \right) \nu, \tag{34}$$

where ν is the outward unit normal to B. This procedure was implemented in [13] and computational results there clearly show that fine details of the shape can be reconstructed provided that the domain is connected.

In the same paper the procedure is applied to detect the domain with multiple components. The results show that the process can create shapes approaching the target shape, but not changing topology. In order to be able to change topology and reconstruct domains with multiple components, we develop a level-set version of the matching GPTs procedure described below.

8.2 Level-set framework

Adopting the level-set framework, one can change the topology in the shape reconstruction. See, for instance, [17,30]. Hence, one can reconstruct the cluster of inclusions $D = \cup_j D_j$ without knowing the number J of separated components of D in advance.
Initial guess: Given $M_{\alpha\beta}$ for $|\alpha| = |\beta| = 1$ (called PT for polarization tensor), one can find an (equivalent) ellipse with the same PT but not its location since the PT is invariant under translation. One can locate this ellipse provided that its GPTs with $|\alpha| + |\beta| = 3$ are known, and it provides a good initial guess. The method is explained in detail in [7] and [13]
Recursive scheme: Within the level set framework, one represents ∂B as the zero level set of a continuous function ϕ so that $B = \{\phi < 0\}$.

As (34), one converts the minimization problem of (31) into a level set form by choosing the gradient ascent direction $V(x)$ on $x \in \partial D_j$ as

$$V(x) = \frac{\mathcal{J}^{(l)}[B]}{\sum_{H,F}\sum_{j=1}^{J'}\left(\langle d_S\mathcal{J}^{(l)}[B], w_j^{HF}[B]\chi_{\partial D_j}\rangle\right)^2}\sum_{H,F}\langle d_S\mathcal{J}^{(l)}[B], w_j^{HF}[B]\chi_{\partial D_j}\rangle w_j^{HF}[B](x), \tag{35}$$

for each $j = 1, \ldots, J'$. We can simply set

$$V(x) = \sum_{H,F}\alpha_j^{HF}[B]w_j^{HF}[B](x), \tag{36}$$

where α_j^{HF} is defined by (35). Then we evolve ϕ by solving the Hamilton–Jacobi equation

$$\frac{\partial\phi}{\partial t} + V|\nabla\phi| = 0, \tag{37}$$

for one time step.

It is worth emphasizing that in (36), V is only defined on the boundary ∂B, even though under the level set framework it has to be defined on the whole domain. Since $\nu = \nabla\phi/|\nabla\phi|$, we can modify w_j^{HF} as

$$\begin{aligned} w_j^{HF}[B]|_- = &\left(k_j + \frac{1}{k_j} - 2\right)\left(\nabla v[B]|_- \cdot \frac{\nabla\phi}{|\nabla\phi|}\right)\left(\nabla u[B]|_- \cdot \frac{\nabla\phi}{|\nabla\phi|}\right) \\ &+ \left(1 - \frac{1}{k_j}\right)\nabla v[B]|_- \cdot \nabla u[B]|_- , \end{aligned} \tag{38}$$

and

$$\begin{aligned} w_j^{HF}[B]|_+ = &-\left(k_j + \frac{1}{k_j} - 2\right)\left(\nabla v[B]|_+ \cdot \frac{\nabla\phi}{|\nabla\phi|}\right)\left(\nabla u[B]|_+ \cdot \frac{\nabla\phi}{|\nabla\phi|}\right) \\ &+ \left(k_j - 1\right)\nabla v[B]|_+ \cdot \nabla u[B]|_+ , \end{aligned} \tag{39}$$

where $u[B]$ and $v[B]$ satisfy (15) and (16), respectively (with D replaced with B). Therefore, the equation (37) for ϕ can be modified as follows:

$$\begin{aligned} &\frac{\partial\phi}{\partial t} + \left(-\operatorname{sgn}(k_j + \frac{1}{k_j} - 2)\left(\nabla v[B] \cdot \frac{\nabla\phi}{|\nabla\phi|}\right)\left(\nabla u[B] \cdot \frac{\nabla\phi}{|\nabla\phi|}\right)\right. \\ &\left. + \frac{1}{2}\left(\operatorname{sgn}(k_j + \frac{1}{k_j} - 2) + (k_j - \frac{1}{k_j})\right)\nabla v[B] \cdot \nabla u[B]\right) = 0 , \end{aligned} \tag{40}$$

where sgn is the sign function.

9 Numerical experiments

In this section, we perform some numerical experiments of recovering the shape of a domain from its GPTs. In all of the numerical examples presented in this section, we apply the level set approach presented in the previous section. We emphasize that we do not make any a priori assumption on the number of connected components of the domain.

In order to acquire the GPTs, we solve the boundary integral equation (1) numerically; see [13] for more detailed explanation. The characteristic size of the inclusions is of order one. All the λ_j are set to be 1 (*i.e.*, $k_j = 3$ for all j assuming that the conductivity of the background is 1) except in Example 6 where the average conductivity is supposed to be known. We use 128 nodal points for solving the integral equation (1). In the level set formulation, we compute the gradient ascent direction V by solving the equations (15) and (16) using a boundary element method. Since the domain is represented implicitly as the zero level set of ϕ, we extract at each step an explicit parametrization of its boundary using a standard segmentation method. The discretization of the boundary is redefined at each step. Again, 128 nodal points are used.

For all the numerical examples below, the separated curves are represented with the same number of discretization points, say M. Except the figures in Example 7, each boundary of a connected inclusion is discretized with $M = 2^7$ number of points. On the other hand, for the Hamilton–Jacobi equation,

$$\frac{\partial \phi}{\partial t} + V|\nabla \phi| = 0,$$

we discretize ϕ and V in the rectangle $[-2, 2] \times [-1, 1]$ on 400×200 grid points with equal spacing, *i.e.* $\Delta x = \Delta y = 0.01$, in all examples except Example 8. Then we have the $(i + 1)$-times iterated solution as

$$\phi^{(i+1)} = \phi^{(i)} - V \Delta t,$$

where $\phi^{(i)}$ is the i-th solution. In all examples except Example 8, we set $\Delta t = 1$.

Example 1 Figure 1 shows that the equivalent ellipse is separated into 2 pieces and gradually modified toward the target domain. The first image is the equivalent ellipse and the others are the reconstructed images after 20, 30, 40, 70, 90 iterations. Figure 2 is the graph of the relative area difference $\frac{|D \triangle B|}{|D|}$, where B is the reconstructed domain.

Example 2 The example in Fig. 3 shows the reconstruction of the 3 inclusions D using $M(1, D) + \mathcal{E}$, instead of $M(1, D)$, with various relative noise $\mathcal{E}$ with

$$\frac{\left(\sum_{|\alpha|+|\beta|\le 6} \left(\sum a_\alpha b_\beta \mathcal{E}_{\alpha\beta}\right)^2\right)^{\frac{1}{2}}}{\left(\sum_{|\alpha|+|\beta|\le 6} \left(\sum a_\alpha b_\beta M_{\alpha\beta}\right)^2\right)^{\frac{1}{2}}} = 0,\ 0.1,\ 0.2.$$

Here we use GPTs up to order 6, *i.e.*, $N = 6$.

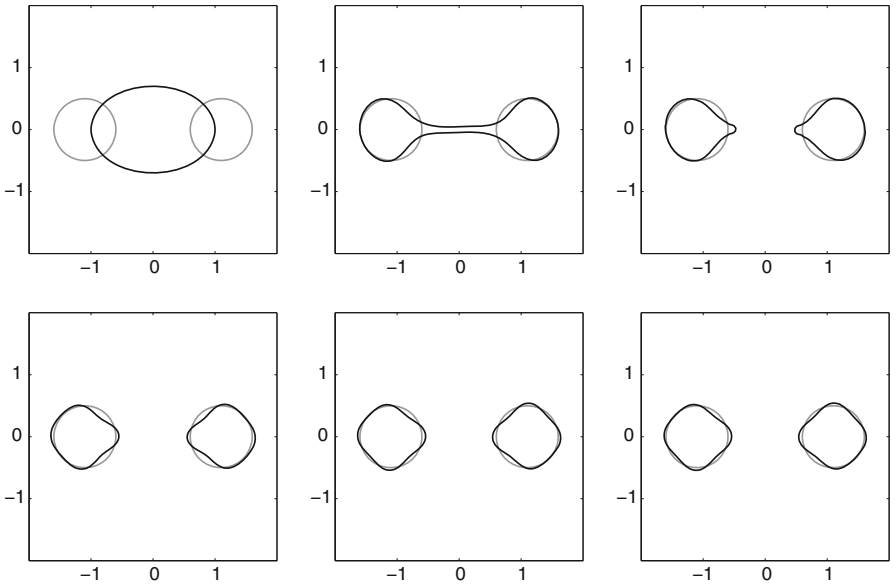

Fig. 1 The GPTs of order $N = 4$, *i.e.*, $M_{\alpha\beta}$ with $2 \leq |\alpha| + |\beta| \leq 4$, separate the inclusion of 2 pieces. The first image is the equivalent ellipse and the others are the reconstructed images after 20, 30, 40, 70, 90 iterations. The *gray curve* is the target domain and the *black curve* is the reconstructed one

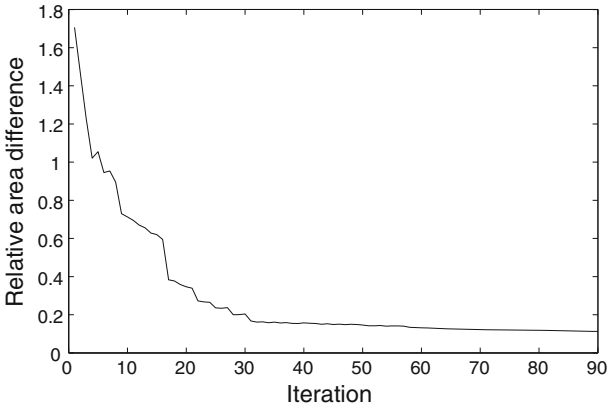

Fig. 2 The relative area difference of the example in Fig. 1

Example 3 This example is to demonstrate that the more components the target has, the higher GPTs are required to separate them. Figure 4 shows that one can not separate two components using $N = 3$, while $N = 4$ can. Similarly, one cannot separate 3 and 4 inclusions using the GPTs of order up to $N = 4$ and $N = 5$, respectively, see Figs. 5 and 6. Figure 7 shows that the GPTs needed to separate multiple inclusions depends on not only the number of inclusions but also their placement. In fact, using GPTs up to $N = 5$ may not be enough to separate 3 inclusions.

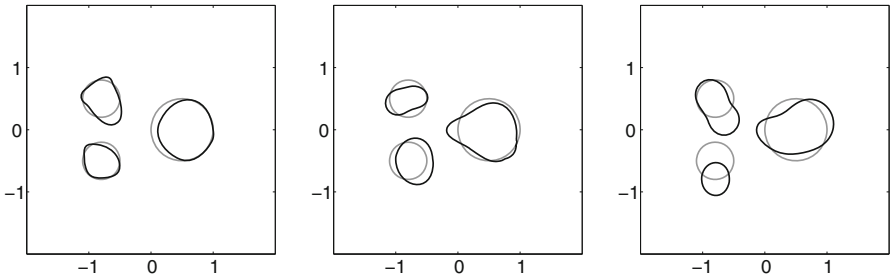

Fig. 3 Reconstructed images after 150 iterations using GPTs of order up to $N = 6$. The first, second and third figure is from the data with 0, 10, 20 % relative noise, respectively

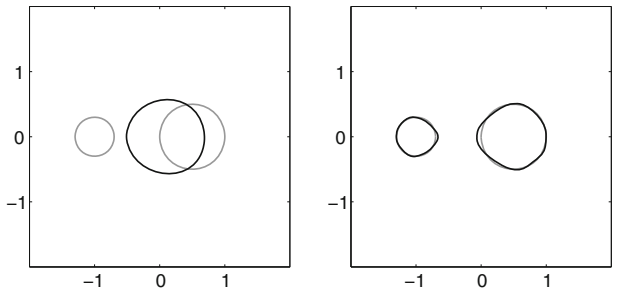

Fig. 4 Reconstructed images after 70 iterations. The first figure is obtained using GPTs of order up to $N = 3$, and the second is of order up to $N = 4$. GPTs of order up to $N = 3$ cannot separate 2 inclusions

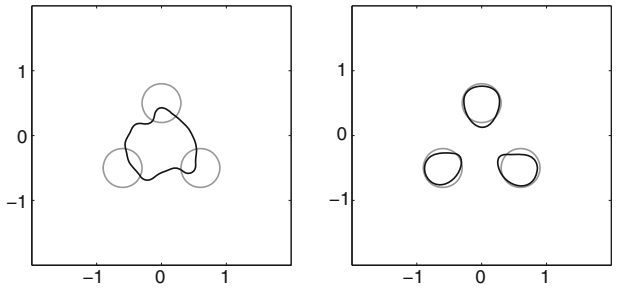

Fig. 5 Reconstructed images after 100 iterations. The first figure is obtained using GPTs of order up to $N = 4$, and the second is of order up to $N = 5$. GPTs of order up to $N = 4$ cannot separate 3 inclusions

Example 4 Figure 8 shows that if two inclusions are located too close, one cannot separate them. It turned out from the numerical simulations that one cannot separate two disks of radius 0.5 using the GPTs of order up to $N = 6$ if the distances between them are smaller than 0.38.

Example 5 High-frequency information is undetectable, see Fig. 9.

Example 6 Even when λ_j of the inclusions D_j are different, one can separate 4 inclusions using the GPTs of order up to $N = 6$ if they have the same signs. In Fig. 10,

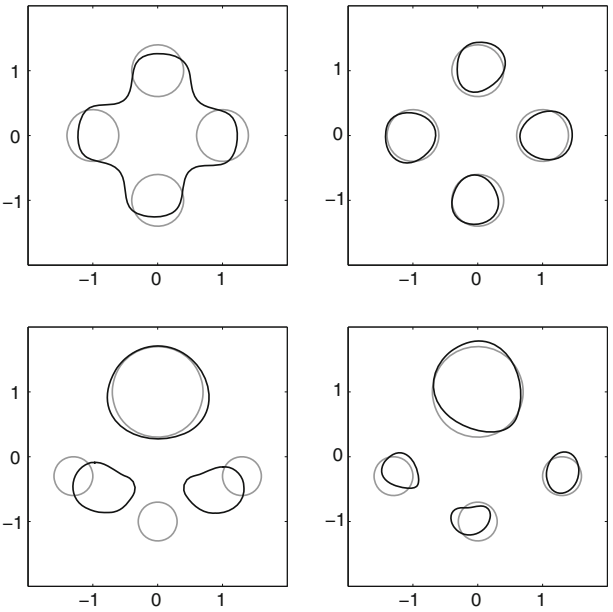

Fig. 6 The first and second columns are reconstructed images after 400 iterations using GPTs of order up to $N = 5$ and $N = 6$, respectively. GPTs of order up to $N = 5$ cannot separate 4 inclusions

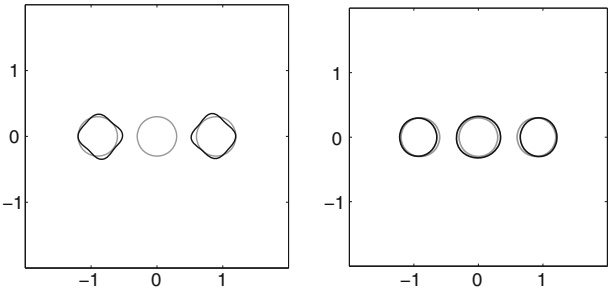

Fig. 7 Reconstructed images after 100 iterations. The first figure is obtained using GPTs of order up to $N = 5$, and the second is of order up to $N = 6$. The number of GPTs needed to separate multiple inclusions depends on not only the number of inclusions but also their placement

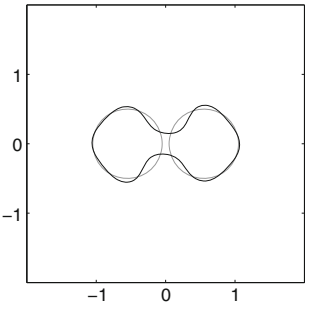

Fig. 8 Reconstructed image after 100 iterations using GPTs of order up to $N = 6$. When two inclusions are located too close, one cannot separate them

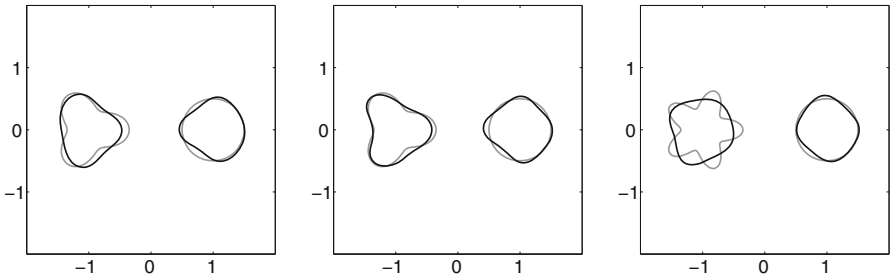

Fig. 9 The first, second, and third figure is the reconstructed image using the GPTs of order up to 4, 5, and 7, respectively. High-frequency (compared to the GPTs order) perturbation is undetectable

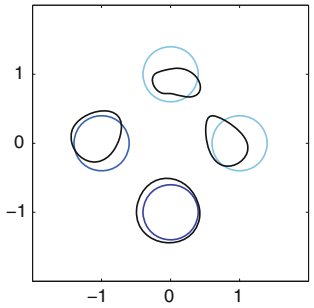

Fig. 10 Reconstructed image after 400 iterations using the GPTs or order up to $N = 6$. The λ_j of *left*, *bottom*, *right*, and *top* inclusions are 1, 1, 11/18, 15/26, respectively

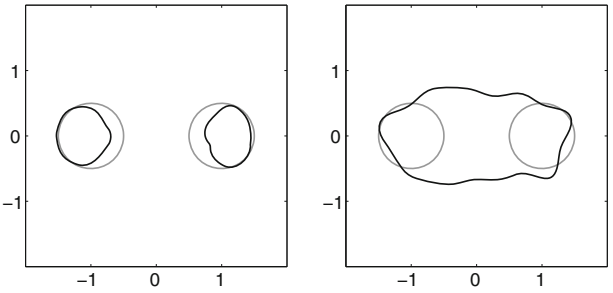

Fig. 11 Reconstruction of two inclusions with $N = 4$ and the same $\lambda = 15/26$ (on the *left*) and $\lambda = 151/298$ (on the *right*) after 250 and 500 iterations, respectively. The topology is not captured for the case with the highest contrast

the λ_j of left, bottom, right, and top inclusions are 1, 1, 11/18, 15/26, respectively. For reconstruction we suppose that the average conductivity is known. In Fig. 11 we consider two inclusions with the same λ and $N = 4$. Figures 10 and 11 show that it is more difficult to reconstruct high contrast inclusions from their GPTs.

If λ_j have different signs, some of them may not be detected. This phenomenon is closely related to our construction of GPTs vanishing structures in [12]. For example, when we reconstruct in Fig. 12 inclusions assuming $\lambda = 1$, the ones with negative λ are undetectable.

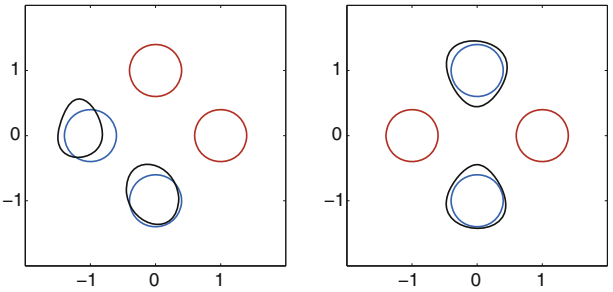

Fig. 12 Reconstructed images after 400 iterations using the GPTs of order up to $N = 6$. The λ_j of *red* and *blue* colors are -1.5, $11/14$, respectively. For reconstruction we use $\lambda = 1$. Inclusions of negative λ are undetectable (color figure online)

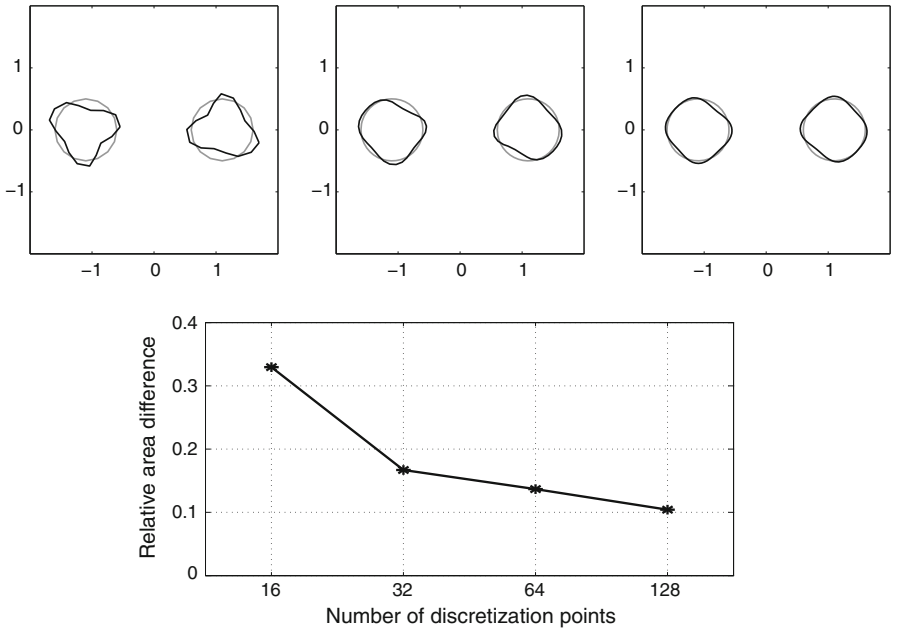

Fig. 13 Reconstruction of 2 inclusions from the GPTs of order $N = 4$, *i.e.*, $M_{\alpha\beta}$ with $2 \leq |\alpha| + |\beta| \leq 4$ after 90 times iteration. The first row is the reconstruction where the number of discretization points is 16, 32 and 64 from the left to the right. The second row is the graph of the relative area difference

Example 7 Figure 13 shows the reconstruction of two inclusions and the relative area difference with various number of discretization points M on one inclusion. The relative area difference after 90 iterations which corresponds to $M = [2^4,\ 2^5,\ 2^6,\ 2^7]$ is $[0.1042,\ 0.1367,\ 0.1670,\ 0.3296]$, respectively. It shows the stability of the reconstruction method with respect to the number of discretization points.

Example 8 In this example, fixing the discretization number on each boundary of inclusion to be $M = 2^7$, we change the time step or the grid point spacing in the

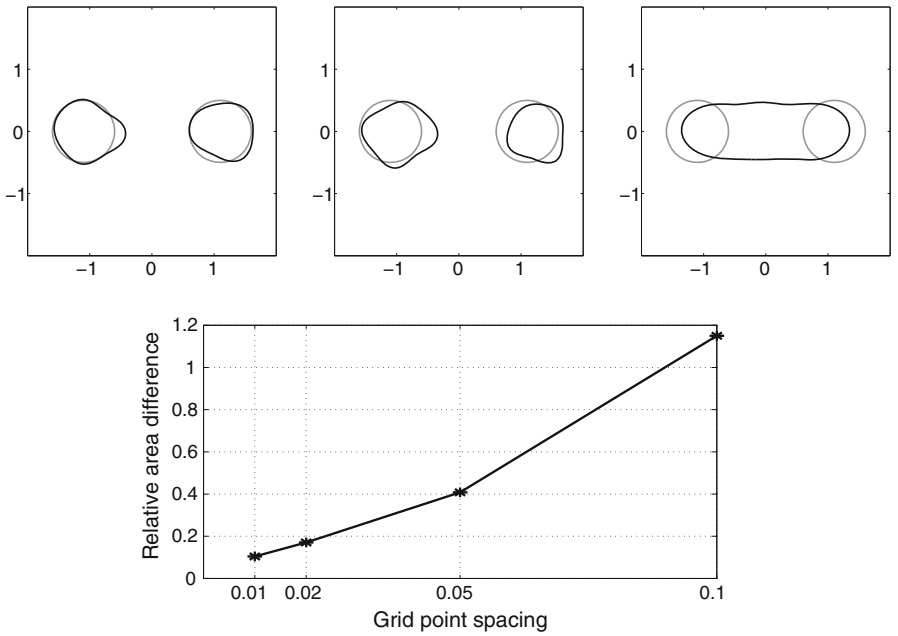

Fig. 14 Reconstruction after 90 iterations of the Example 1 with various grid point spacings in the Hamilton–Jacobi equation. The first row is the reconstruction where the grid point spacing $\Delta x = \Delta y$ is 0.02, 0.05, and 0.1 from the left to the right. The second row is the graph of the relative area difference

Hamilton–Jacobi equation in the Example 1. When we use the time step $\Delta t = 2$ and 5, the relative area difference after 90 iterations are 0.1108 and 0.1596, respectively. But for $\Delta t = 8$, the iteration solution does not converge. Figure 14 shows the reconstruction with various grid point spacings. The relative area difference corresponds to $\Delta x = \Delta y = [0.01, 0.02, 0.05, 0.1]$ is $[0.1042, 0.1705, 0.4083, 1.1505]$, respectively.

10 Conclusion

In this paper we have presented a new approach for shape description and matching. Our approach is based on a novel global shape descriptor, the notion of GPTs. Compared to moments, which provide a region descriptor, the GPTs can be viewed as a boundary descriptor. We have performed numerical simulations to demonstrate that GPTs capture both high frequency shape oscillations and topology.

Moreover, the notion of GPTs gives a natural hierarchical shape distance. The discrepancy between the contracted GPTs, M^c_{mn} for $m, n \leq N$, associated to two clutters of inclusions measure the similarity between them. Higher is N, better is the correspondence between the high-frequency details in the two clutters. This will be used in a forthcoming work for target recognition from wave imaging data.

As shown in [14], GPTs can be accurately obtained from (multistatic) wave measurements by solving a linear system. Therefore, it would be very interesting in wave

imaging to design a fast algorithm which identifies a target using a dictionary of pre-computed GPTs data. Very recently, this approach has been successfully implemented for conductivity imaging based on new invariants for the GPTs [1].

Another challenging problem is to understand the relationship between the number of connected components of a target and the number of GPTs needed to separate them. Formula (30) can be used as an indicator of topology if the GPTs we have in hand are for λ close to $1/2$. However, in the general case the question seems to be very difficult. The particular case of multiple disk-shaped inclusions could be handled explicitly. It would be very interesting to find a formula for the number of GPTs needed to separate multiple disk-shaped inclusions as function of their number, radii, and the distances between them.

References

1. Ammari, H., Boulier, T., Garnier, J., Jing, W., Kang, H., Wang, H.: Target identification using dictionary matching of generalized polarization tensors. (Submitted)
2. Ammari, H., Ciraolo, G., Kang, H., Lee, H., Milton, G.: Spectral theory of a Neumann–Poincaré-type operator and analysis of cloaking due to anomalous localized resonance. Arch. Rat. Mech. Anal. **208**, 667–692 (2013)
3. Ammari, H., Ciraolo, G., Kang, H., Lee, H., Yun, K.: Spectral analysis of the Neumann–Poincaré operator and characterization of the gradient blow-up. Arch. Rat. Mech. Anal. **208**, 275–304 (2013)
4. Ammari, H., Garnier, J., Sølna, K.: Resolution and stability analysis in full-aperature, linearized conductivity and wave imaging. Proc. Am. Math. Soc. (To appear)
5. Ammari, H., Kang, H.: High-order terms in the asymptotic expansions of the steady-state voltage potentials in the presence of conductivity inhomogeneities of small diameter. SIAM J. Math. Anal. **34**, 1152–1166 (2003)
6. Ammari, H., Kang, H.: Properties of generalized polarization tensors. SIAM Multiscale Model. Simul. **1**, 335–348 (2003)
7. Ammari, H., Kang, H.: Reconstruction of small inhomogeneities from boundary measurements. In: Lecture Notes in Mathematics, vol. 1846. Springer, Berlin (2004)
8. Ammari, H., Kang, H.: Boundary layer techniques for solving the Helmholtz equation in the presence of small inhomogeneities. J. Math. Anal. Appl. **296**, 190–208 (2004)
9. Ammari, H., Kang, H.: Polarization and moment tensors with applications to inverse problems and effective medium theory. In: Applied Mathematical Sciences, vol. 162. Springer, New York (2007)
10. Ammari, H., Kang, H., Kim, E., Lim, M.: Reconstruction of closely spaced small inclusions. SIAM J. Numer. Anal. **42**, 2408–2428 (2005)
11. Ammari, H., Kang, H., Lim, M.: Polarization tensors and their applications. In: Proceedings of the second International Conference on Inverse Problems: recent developments and numerical approaches, Shanghai, 2004. J. Phy. Conf. Ser. **12**, 13–22 (2005)
12. Ammari, H., Kang, H., Lim, M., Lee, H.: Enhancement of near-cloaking using generalized polarization tensors vanishing structures. Part I: the conductivity problem. Comm. Math. Phys. **317**, 253–266 (2013)
13. Ammari, H., Kang, H., Lim, M., Zribi, H.: The generalized polarization tensors for resolved imaging. Part I: shape reconstruction of a conductivity inclusion. Math. Comp. **81**, 367–386 (2012)
14. Ammari, H., Kang, H., Kim, E., Lee, J.-Y.: The generalized polarization tensors for resolved imaging. Part II: shape and electromagnetic parameters reconstruction of an electromagnetic inclusion from multistatic measurements. Math. Comp. **81**, 839–860 (2012)
15. Ammari, H., Kang, H., Nakamura, G., Tanuma, K.: Complete asymptotic expansions of solutions of the system of elastostatics in the presence of inhomogeneities of small diameter. J. Elast. **67**, 97–129 (2002)
16. Ammari, H., Kang, H., Touibi, K.: Boundary layer techniques for deriving the effective properties of composite materials. Asymp. Anal. **41**, 119–140 (2005)
17. Burger, M., Osher, S.J.: A survey on level set methods for inverse problems and optimal design. Eur. J. Appl. Math. **16**, 263–301 (2005)

18. Capdeboscq, Y., Karrman, A.B., Nédélec, J.-C.: Numerical computation of approximate generalized polarization tensors. Appl. Anal. **91**, 1189–1203 (2012)
19. Capdeboscq, Y., Vogelius, M.S.: A general representation formula for the boundary voltage perturbations caused by internal conductivity inhomogeneities of low volume fraction. Math. Model. Num. Anal. **37**, 159–173 (2003)
20. Cedio-Fengya, D.J., Moskow, S., Vogelius, M.S.: Identification of conductivity imperfections of small diameter by boundary measurements: continuous dependence and computational reconstruction. Inverse Probl. **14**, 553–595 (1998)
21. Dassios, G., Kleinman, R.: Low frequency scattering. In: Oxford Mathematical Monographs. Oxford University Press, New York (2000)
22. Folland, G.B.: Introduction to Partial Differential Equations. Princeton University Press, Princeton (1976)
23. Friedman, A., Vogelius, M.S.: Identification of small inhomogeneities of extreme conductivity by boundary measurements: a theorem on continuous dependence. Arch. Rat. Mech. Anal. **105**, 299–326 (1989)
24. Goldenshluger, A., Spokoiny, V.: On the shape-from-moments problem and recovering edges from noisy Radon data. Prob. Theory Relat. Fields **128**, 123–140 (2004)
25. Goldenshluger, A., Zeevi, A.: Recovering convex boundaries from blurred and noisy measurements. Ann. Stat. **34**, 1375–1394 (2006)
26. Khavinson, D., Putinar, M., Shapiro, H.S.: Poincaré's variational problem in potential theory. Arch. Ration. Mech. Anal. **185**, 143–184 (2007)
27. Loncaric, S.: A survey of shape analysis techniques. Pattern Recognit. **31**, 983–1001 (1998)
28. Milton, G.W.: The theory of composites. In: Monographs on Applied and Computational Mathematics. Cambridge University Press, Cambridge (2001)
29. Pólya, G., Szegö, G.: Isoperimetric inequalities in mathematical physics. In: Annals of Mathematical Studies, vol. 27. Princeton University Press, Princeton (1951)
30. Santosa, F.: A level-set approach for inverse problems involving obstacles. ESAIM COCV **1**, 17–33 (1996)
31. Teague, M.R.: Image analysis via the general theory of moments. J. Opt. Soc. Am. **70**, 920–930 (1980)